The Pharmacokinetics of [18F]UCB-H Revisited in The Healthy Non-Human Primate Brain

Sébastien Goutal
CEA Paris-Saclay Center - Fontenay-aux-Roses Site: Commissariat a l'energie atomique et aux energies alternatives Site de Fontenay-aux-Roses
Martine Guillermier
CEA Paris-Saclay Center - Fontenay-aux-Roses Site: Commissariat a l'energie atomique et aux energies alternatives Site de Fontenay-aux-Roses
Guillaume Becker
Université de Liège
Mylène Gaudin
CEA Paris-Saclay Center - Fontenay-aux-Roses Site: Commissariat a l'energie atomique et aux energies alternatives Site de Fontenay-aux-Roses
Yann Bramoullé
CEA Paris-Saclay Center - Fontenay-aux-Roses Site: Commissariat a l'energie atomique et aux energies alternatives Site de Fontenay-aux-Roses
André Luxen
Université de Liège: Universite de Liege
Christian Lemaire
Université de Liège: Universite de Liege
Alain Plenevaux
Université de Liège: Universite de Liege
Eric Salmon
University of Liege: Universite de Liege
Philippe Hantraye
CEA Paris-Saclay Center - Fontenay-aux-Roses Site: Commissariat a l'energie atomique et aux energies alternatives Site de Fontenay-aux-Roses
Olivier Barret
CEA Paris-Saclay Center - Fontenay-aux-Roses Site: Commissariat a l'energie atomique et aux energies alternatives Site de Fontenay-aux-Roses
Nadja Van Camp (✉ nadja.van-camp@cea.fr)
CEA Paris-Saclay Center - Fontenay-aux-Roses Site: Commissariat a l'energie atomique et aux energies alternatives Site de Fontenay-aux-Roses https://orcid.org/0000-0002-2261-7314

Original research

Keywords: SV2A, cynomolgus non-human Primates, PET, Synaptic imaging

Posted Date: November 20th, 2020

DOI: https://doi.org/10.21203/rs.3.rs-110220/v1

Version of Record: A version of this preprint was published at EJNMMI Research on April 7th, 2021. See the published version at https://doi.org/10.1186/s13550-021-00777-8.

Abstract

Background Positron Emission Tomography (PET) imaging of the Synaptic Vesicle glycoprotein (SV) 2A is a new tool to quantify synaptic density. [18F]UCB-H was one of the first promising SV2A-ligands to be labelled and used *in vivo* in rodent and human, while limited information on its pharmacokinetic properties is available in the non-human primate. Here, we aimed to characterize [18F]UCB-H in the non-human cynomolgus primate and to discuss the obtained results in the light of the current state of SV2A PET ligands.

Results [18F]UCB-H pharmacokinetic data was optimally fitted with a two-compartment model (2TCM), even though a slow component led to instability for the estimation of k_3 and k_4, and hence the total volume of distribution. 2TCM with coupled fit K_1/k_2 across brain regions stabilized the quantification, and confirmed a lower non-displaceable binding potential, BP_{ND} (estimated by k_3/k_4), of [18F]UCB-H compared to the newest SV2A-ligands. However, the non-displaceable distribution volume (V_{ND}) and the influx parameter (K_1) is similar to what has been reported for other SV2A ligands. These data were reinforced by displacement studies using [19F]UCB-H, demonstrating only 50 % displacement of the total [18F]UCB-H signal at maximal occupancy of SV2A.

Conclusions Modeling issues with a 2TCM due to a slow component have previously been reported for other SV2A ligands with low specific binding, or after blocking of specific binding. As all SV2A ligands share chemical structural similarities, we hypothesize that this slow binding component is common for all SV2A ligands, but only hampers quantification when specific binding is low.

Background

Synaptic vesicle glycoproteins (SV) are critical to proper nervous system function and have been demonstrated to be involved in vesicle trafficking. They belong to the Major Facilitator Superfamily (MFS) of transporters and consist of a 12-transmembrane glycoprotein and a cytoplasmic N-terminal region containing a long sequence that varies among the three SV2 isoforms (SV2A, SV2B and SV2C) (1, 2). SV2A and -B are highly homologous to each other, with SV2A showing ubiquitous expression in both excitatory and inhibitory synapses throughout the entire brain (3, 4); in contrast, SV2B and SV2C are present in a more restricted pattern in the brain, and in only a subset of synapses (2, 5). The hypothesis of SV2 as vesicular transport protein is based on a significant homology to other transport proteins, however no endogenous substrate has been reported (3), neither has any transport activity been demonstrated (2). Another hypothetical function is vesicle trafficking and exocytosis, and the modification of the synaptic function (4–6).

Lynch and coworkers identified SV2A as the brain-binding site of the anti-epileptic drug levetiracetam (LEV, Keppra®, UCB Pharma Ltd., Slough, Berkshire, UK) (7). Seizure protection by LEV and other SV2A ligands strongly correlates with the degree of SV2A occupancy in *vivo* (3, 8). However, the site of SV2A-LEV interaction and the mechanism of action remain unclear. LEV does not cause a SV2A conformational state change and it is assumed that SV2A transports LEV or LEV prevents transport of the endogenous substrate (4), as one of the functional consequences of LEV binding to SV2A in brain slices is reduced exocytosis (6). With the aim of a better understanding of the role of SV2A in epilepsy and of studying SV2A in diseases of the central nervous system, several SV2A-specific ligands have been developed (9), [18F]UCB-H being one of the first to be labelled (10), subsequently characterized in the rodent (10, 11), and in the human brain (12). The demonstration of the co-localization of SV2A with other synaptic markers using [11C]-UCB-J (13), showed the potential of *in vivo* imaging of the synaptic density using Positron Emission Tomography (PET), and led recently to the development of new 18F-labelled ligands (9, 14–19). Preclinical characterization of [18F]UCB-H has mostly been done in the rodent brain (20–22), while in non-human primates (NHP) limited data is available (23, 24). In humans a preliminary study was performed on four healthy subjects (12), preceding a clinical study in Alzheimer's patients (25). Here, we aimed to characterize pharmacodynamics properties of [18F]UCB-H in non-human cynomolgus primates in complement to these existing data and to discuss the obtained results in the light of the current state of SV2A PET ligands.

Material And Methods

Animals

Experiments were conducted on four young adult male cynomolgus monkeys (Macaca fascicularis, 5.2 ± 1.1 kg, 4.4 ± 0.7 years). Animal use procedures were in accordance with the recommendations of the European regulations (EU Directive 2010/63) and approved by the local ethical committee (CETEA n°44), and the French Ministry of Education and Research (NEUROMODEL: APAFIS#389-2015032716213569 0v02). The experimental data reported in this study are in compliance with the ARRIVE (Animal Research: Reporting in Vivo Experiments) guidelines (26).

Radiochemistry

Radiosynthesis of the enantiomeric ligand [18F]UCB-H was realized through a one-step radiolabelling of a pyridyliodonium precursor as previously described (27). [18F]UCB-H was formulated in 0.9% aqueous saline with 3% ethanol (v/v). The radiochemical purity of [18F]UCB-H was > 98% and the molar activity at the time of injection was 54±32 GBq/µmol.

PET Imaging

Experimental Design - All four non-human primates (NHP) underwent a 2-hour (2hr) test and retest PET scan; two NHP underwent an additional 4hr retest PET scan. Three NHP underwent one 4-hour (4hr) displacement PET scan. Arterial blood sampling was performed during test and retest scans with PET imaging spaced by at least 3 weeks between each scan. To this end, the femoral artery opposite to the saphenous vein used for radioligand injection was cannulated. For the 2hr scans, we collected in total 28 blood samples of 1 mL: 16 samples during the first 5 minutes followed by 3 samples every 5 minutes and 11 samples every 10 minutes. For the 4hr scans, we collected an additional 6 samples every 20 minutes during the last two hours (34 samples in total). Larger samples (2 – 3 mL) were collected at 5, 15, 30, 60, 90, 120 minutes (2hr) and at 180, 240 minutes (4hr) for metabolite analysis. Displacement of [18F]UCB-H was done by intravenous (IV) administration 90 minutes after [18F]UCB-H injection of a bolus of 30 mg/kg LEV, or of 80 µg/kg (≈250 nmol/kg) or 5 mg/kg (≈15 µmol/kg) of cold [19F]-UCB-H.

Drug Formulation - Solvents and LEV ($C_8H_{14}N_2O_2$; MM 170.21 g/mol) were obtained at Sigma-Aldrich® (France), and [19F]-UCB-H ($C_{16}H_{12}F_4N_2O$; MM 324.28 g/mol) was synthesised as previously described (27). Injectable solutions of [19F]-UCB-H for displacement studies were prepared with a mixture of Tetrahydrofuran (THF), Médialipide® and glucose at 2.5% as previously described (28). LEV was dissolved in a glucose solution of 2.5% to reach a concentration of 90 mg/mL.

PET imaging – PET imaging was performed on the microPET FOCUS220 (Siemens) under standard anesthesia and monitoring procedures (29). Data acquisition started with the IV bolus injection of [18F]UCB-H (32.9±1.0 MBq/kg, 0.35±0.07 µg/kg). Dynamic PET images were reconstructed using standard OSEM-2D algorithms while correcting for radioactive decay, scatter, attenuation and detectors inhomogeneity, which were measured prior to PET scanning using respectively ^{57}Co and ^{68}Ge external sources.

Blood Measurement & Analysis - Plasma was separated from whole-blood by centrifugation (5 minutes, 2054xg, 4°C) and 50 µL of plasma and whole-blood were counted using a PET cross-calibrated gamma well counter (WIZARD^2, PerkinElmer, France) to obtain the whole-blood and plasma activity curves. All data were corrected for radioactive decay from the injection time. For the larger blood samples, 500 µL plasma was deproteinized with acetonitrile. The supernatant was injected in high-performance liquid chromatography, equipped with an Atlantis® T3 5µm 4.6x150mm column (Waters) and an Atlantis® T3 5µm 3.9x5mm pre-column (Waters), with an LB-513 radioactivity flow detector (Berthold, La Garenne Colombes, France, MX Z100 cell). The eluant was collected in interval of 15 seconds (fraction collector III, Waters, France) and counted in the gamma well counter (WIZARD^2, PerkinElmer, France) to measure total activity. The unmetabolized parent [18F]UCB-H was calculated as a percentage of the total radioactivity (metabolites and parent).

For each animal, a 2-exponential decay function was fitted to the parent fraction of [18F]UCB-H , which was time multiplied with the plasma activity curve to obtain the metabolite-corrected arterial plasma input function (mcAIF) used for the kinetic modeling.

The fraction of [18F]UCB-H in NHP plasma samples not bound to plasma protein was measured before PET injection using a previously described ultrafiltration method (30). In brief, standard amounts of [18F]UCB-H (≈15 kBq) were added to 200 µL plasma that was applied to Microcon® filtration devices containing an YM-10 membrane (Millipore, France). The devices were centrifuged for 10 min at 10000 g (Sigma 2-16KL, France). [18F]UCB-H activity concentration in the resulting ultrafiltrate (≈70 µL, CFP) and a sample of plasma (CP) were counted. The free fraction (f_p) was calculated as: f_p=CFP/CP and measured in triplicates.

PET data analysis – PET image analysis was performed using PMOD software version 3.8 (PMOD Technologies Ltd., Zurich, Suisse). After individual co-registration of PET-MR images, a cynomolgus atlas published by Ballanger and coworkers (31) was normalized to PET images to extract time activity curves in different brain regions. Volumes of interest (VOI) were cerebral white matter, striatum, thalamus, cerebellum, frontal -, parietal -, and temporal cortex, and whole brain as a composite region of all regions in the atlas. [18F]UCB-H pharmacokinetics were evaluated by analyzing the time activity curves of the test- and retest scans using 1- and 2-tissue compartment models (unconstrained and constrained with global K_1/k_2 coupled fit across all regions) (32), and Logan graphical analysis with a fixed t* at 60 minutes (33) using the arterial plasma input function corrected for radio-metabolites to derive the volume of distribution in each region. Percentage standard error (%SE) was estimated from the theoretical parameter covariance matrix. Only V_T and k_3/k_4 values with reliably estimates, i.e. %SE less than 25%, were included in the current analyses. For the three drug studies, percent displacement of the total activity in the whole brain was estimated relative to an average baseline constructed from the two 4hr baseline studies. The curves of the average baseline and the three displacement studies were normalized by the activity immediately before the administration of the drugs. The percent displacement of total activity was then calculated as (baseline-displacement)/baseline.

Statistical Analysis – Statistical analysis was performed using R software (version 3.3.1.). Plasma, intact parent fraction and time activity curves were statistically compared between subjects using a one-factor variance analysis. *Absolute Test-Retest variability* (aTRV) of PET quantification parameters was calculated as ABS(test - retest) / AVERAGE(test , retest). All values are expressed as average ± standard error of the mean (SEM; significance level was fixed at $p < 0.05$).

Results

Blood data

[18F]UCB-H shows a rapid metabolism in the arterial blood with an intact parent fraction of 37 ± 3.9% at 15 min, 29.5 ± 3.4% at 30 min, 19 ± 3.5% at 60 min, 14.6 ± 1.9% at 120 minutes and 4.4 ± 0.7% at 240 min after tracer injection. The parent fraction was fitted with a two-exponential decay function based on blood data acquired up to 4h after tracer injection, and on the residuals (**Figure 1A**). Whole blood and plasma-input functions were highly consistent between animals with stable plasma to whole-blood ratio of 0.90 ± 0.05 over the entire 120-minute acquisition period (**Figure 1B-C**). Plasma free parent fraction (f_p) measured by ultrafiltration before tracer injection was 42.6 ± 1.6 %.

Brain kinetics

Time Activity curves - Figure 2B shows representative time-activity curves (TACs) in a subset of brain regions. [18F]UCB-H entered rapidly in the brain, reaching maximal uptake 5 to 15 minutes after injection, followed by a relatively slow terminal elimination phase. Highest standardized uptake value (SUV) uptake was observed in the striatum, followed by the thalamus and the cortical regions.

Compartment modeling - According to the lowest Akaike Information Criterion (AIC), the two-compartment model (2TCM) fitted better the TACs compared to the one-compartment model (1TCM) (AIC_{1TCM} = 21.9 ± 1.8 *vs.* AIC_{2TCM} = 0.71 ± 1.73). 1TCM was not sufficient to describe adequately the TACs with a classic overestimation of the medial part and underestimation of the terminal part of the TAC (**Figure3A)**. However, across all scans and VOI, V_T estimated by 2TCM was only quantifiable in 50 % of cases. There was high uncertainty on the estimation of k_3 and even higher for k_4 where the estimate tended toward 0 in more than 30% of cases independent of the VOI. As a result, reliable estimates of k_3/k_4 were only obtained in 20 % of cases. 2TCM with coupled fit K_1/k_2 across brain regions was more stable and enabled estimation of V_T in 80% of cases, and of k_3/k_4 in 70% of cases. Logan graphical analysis fitted robustly all TACs, with a representative plot shown in **Figure 3B**.

Figure 4A shows a comparison between 2TCM and 1TCM and Logan V_T estimates for the cases when 2TCM converged. Good agreement (R^2 = 0.90) was found between 2TCM and Logan estimates with a slight overall underestimation of V_T (-3 ± 1%), while 1TCM had a moderate correlation with 2TCM (R^2 = 0.68) and overall larger bias V_T (-9 ± 1%) (**Figure4B)**.

A summary of V_T obtained by the different methods (2TCM, 2TCM with coupled fit, 1TCM and Logan) and k_3/k_4 (obtained by 2TCM with coupled fit K_1/k_2) for different regions is shown in **table 1**, along with V_T and k_3/k_4 aTRV assessment in **table 2**. As surrogate of BP_{ND}, k_3/k_4 was estimated to be 1.07±0.02 on average, with a not too surprising high aTRV (> 20%). The tissue influx parameter of [18F]UCB-H (K_1), a measure of blood flow and tracer extraction, was equal for 2TCM and 2TCM coupled fit and estimated to 0.37 ± 0.01 mL/cm^3/min in grey matter regions. The average V_{ND} (K_1/k_2 from 2TCM coupled fit) over all VOIs and animals was 7.89 ± 1.23 mL/cm^3, with a free fraction in tissue f_{ND} of 6.1 ± 1.3%.

Table 1- Summary of V_T- and BP_{ND} estimates

	2TCM			2TCM, K_1/k_2 coupled			1TCM			Logan (t*=60)			2TCM, K_1/k_2 coupled		
	V_T [mL/cm^3]			V_T [mL/cm^3]			V_T [mL/cm^3]			V_T [mL/cm^3]			k_3/k_4 (BP_{ND})		
Brain region	**Mean**	**±**	**SEM**	**Mean**	**±**	**SEM**	**Mean**	**±**	**SEM**	**Mean**	**±**	**SEM**	**Mean**	**±**	**SEM**
Striatum															
Test	15,3	±	2,25	15,0	±	1,11	14,2	±	1,29	15,8	±	1,15	1,16	±	0,36
Retest	14,1	±	0,96	15,3	±	0,93	14,8	±	0,61	15,7	±	1,04	1,12	±	0,39
Thalamus															
Test	15,6	±	1,98	15,0	±	1,38	13,3	±	1,17	14,9	±	0,99	1,03	±	0,25
Retest	13,0	±	1,08	14,2	±	1,06	13,4	±	0,60	14,3	±	1,11	0,97	±	0,36
Cerebellum															
Test	10,6	±	0,08	9,70	±	*NA*	9,8	±	0,78	11,2	±	0,68	1,24	±	*NA*
Retest	12,3	±	*NA*	13,3	±	2,97	10,4	±	0,82	11,1	±	0,75	1,22	±	0,42
White Matter															
Test	14,0	±	2,37	13,8	±	1,69	12,3	±	1,13	13,9	±	1,00	1,25	±	0,16
Retest	12,6	±	1,08	13,7	±	1,61	12,5	±	0,68	13,6	±	1,23	0,83	±	0,47
Frontal Cortex															
Test	16,3	±	3,68	14,8	±	2,15	13,8	±	1,64	15,0	±	1,59	1,25	±	0,32
Retest	13,1	±	0,66	14,7	±	1,37	13,8	±	1,15	14,8	±	1,87	1,32	±	0,40
Temporal Cortex															
Test	13,9	±	1,60	14,8	±	1,30	12,9	±	0,83	14,1	±	0,77	1,00	±	0,24
Retest	14,0	±	0,01	13,1	±	0,76	13,0	±	0,52	13,9	±	0,91	0,97	±	0,54
Parietal Cortex															
Test	15,5	±	3,24	15,4	±	1,54	14,3	±	1,41	15,4	±	1,35	1,08	±	0,26
Retest	13,6	±	0,36	16,1	±	1,40	14,8	±	0,75	15,7	±	1,43	1,17	±	0,29

V_T was estimated using 2TCM, 2TCM with K_1/k_2 coupled over all regions, 1TCM and Logan. BP_{ND} was estimated by k_3/k_4 using a 2TCM with K_1/k_2 coupled over all regions. Only estimates at <25%SE were included. NA = undetermined.

Table2: Summary of aTRV

	2TCM	2TCM, K_1/k_2 coupled		1TCM	Logan (t*=60)
Brain region	V_T [mL/cm^3]	V_T [mL/cm^3]	k_3/k_4 (BP_{ND})	V_T [mL/cm^3]	V_T [mL/cm^3]
Striatum	14%*	12%	20%	10%	11%
Thalamus	3%*	18%	27%	13%	12%
Cerebellum	14%*	*NA*	28%	10%	14%
White Matter	10%*	24%	22%	12%	13%
Frontal Cortex	13%*	11%	28%	12%	11%
Temporal Cortex	13%*	25%	36%	12%	13%
Parietal Cortex	13%*	19%	36%	14%	12%

*V_T was obtained with 2TCM, 2TCM with K_1/k_2 coupled over all regions, 1TCM and Logan; BP_{ND} was estimated by k_3/k_4 using a 2TCM with K_1/k_2 coupled over all regions. Only estimates at <25%SE were included. *aTRV could only be estimated from one NHP. NA = undetermined.*

Displacement studies

In all brain regions, [18F]UCB-H uptake was displaced by [19F]UCB-H in a dose-dependent manner with the displacement occurring rapidly; brain penetration of [19F]UCB-H is fast with maximum uptake 5-15 min after injection. Low dose of [19F]UCB-H (80 µg/kg, more than 100 fold [18F]UCB-H mass dose) resulted in ~20-25% displacement, and high dose of [19F]UCB-H (5 mg/kg) displaced close to 50% of [18F]UCB-H, where both measurements were estimated at 35 minutes after injection of cold [19F]UCB-H when the displacement was maximum (**Figure 3C**).

LEV administration at pharmacological dose has a much slower brain penetration ((34)), and a dose of 30 mg/kg induced a slower displacement of [18F]UCB-H of ~40% as estimated at 150 min after injection of LEV (at the end of the 240 min acquisition) (**Figure 3C**).

Discussion

The current study evaluates [18F]UCB-H pharmacokinetics in healthy NHPs. We demonstrated similar metabolism in NHP as previously described in the rodent, human and rhesus monkey (11, 12, 23). We have shown that [18F]UCB-H equilibrates rapidly between whole blood and plasma, with high availability in plasma (f_p of 42.6 ± 1.6%). Similar to data obtained in rodent and human (11, 12), we observed in the NHP a good brain penetrance with ubiquitous brain uptake. Tissue influx parameters of [18F]UCB-H were comparable to other SV2A radioligands for grey matter regions (13, 24). In contrast to preliminary NHP data (23), but coherent with clinical data (12), a better goodness of fit of the TACs was obtained with 2TCM compared to 1TCM, though not all TACs could be fitted with 2TCM. We observed that this convergence issue was mainly due to instability of the k_4 estimate tending to zero in ~ 30% of cases, independent of the regions. Due to these modelling difficulties with 2TCM, the graphical method of Logan was previously suggested to estimate V_T in all brain regions (12). Here, we demonstrate that Logan provides reliable estimates of V_T with a relatively low aTRV (~ 12%), although larger than that reported for [11C]UCB-J in humans (~ 4%)(35), and a small bias relative to 2TCM of ~-3% compared to ~-9% for 1TCM. In a previous rhesus NHP study, Zheng and colleagues alternatively proposed the multilinear analysis method (MA1) to obtain reliable estimates of V_T (23) for [18F]UCB-H. We explored this method and found that the aTRV of V_T (~ 11%) was comparable to Logan, but that the negative bias (~-8%) was larger (*data not shown*).

Brain kinetics of SV2A ligands [11C]UCB-J (35, 36) and [18F]SynVesT-1 (a.k.a [18F]SDM-8, [18F]MNI-1126) (14) have been reported as better described by 2TCM in human, but were better modeled with 1TCM in cynomolgus or rhesus monkeys (24, 37, 38), and [11C]UCB-A was better described with 1TCM at baseline in pigs but 2TCM was required after blocking of the specific signal (39). Interestingly, all authors reported issues with 2TCM similar to those reported here, namely lack of convergence or large standard error for V_T (14, 35, 36, 39), with large uncertainty on k_4 and values close to 0 (14, 35). As a consequence, 1TCM for [11C]UCB-J and [18F]SynVesT-1 (14, 35), and Logan graphical analysis for [11C]UCB-A (39) was selected to as method of choice. Our results suggest a small very slow component for [18F]UCB-H, the nature of which remains unclear. Given the similarity in chemical structures between the current SV2A ligands and the aforementioned results reported in the literature, we hypothesize that this slow component is likely common between all these ligands. This component only hampers 2TCM estimation, and is problematic when the specific signal is low (low affinity ligands or blocking studies) where 2TCM is required because 1TCM does not adequately describe the kinetics.

This was nicely illustrated with [18F]MNI-1126 (high affinity of the (*R*)-enantiomer), [18F]MNI-1038 (racemate) and [18F]MNI-1128 (low affinity of the (*S*)-enantiomer) (24, 40), where 1TCM was the best model for [18F]MNI-1126, but 2TCM had to be used both for [18F]MNI-1038 and [18F]MNI-1128 (lower specific signal), with very low k_4 for [18F]MNI-1128 (24). Here, similarly to [11C]UCB-A (39), the method of choice for [18F]UCB-H was Logan graphical analysis, as 1TCM was not adequate due to its lower affinity compared to other SV2A radioligands.

Quasi-irreversibility of the kinetics was sometimes observed (k_4 close to 0). Therefore, we performed homologous (with [19F]UCB-H) and heterologous (with reference compound LEV) displacement studies to evaluate the reversibility of [18F]UCB-H binding. The total uptake of [18F]UCB-H was clearly displaceable, and in a dose-dependent manner by [19F]UCB-H up to 50% of the total uptake at the highest dose tested (5 mg/kg). Based on [18F]UCB-H brain uptake curves and an f_{ND} of ~ 6%, we have a maximum free concentration of UCB-H of ~ 2.5 mM after administration 5.0 mg/kg. For UCB-H, in vitro K_i of 9 nM in human brain (40) and in vivo K_D of 30 nM in NHP (38) were reported, and conservatively considering a K_D of 30 nM, near full saturation of SV2A would be expected (> 98% occupancy) at a dose of 5 mg/kg and a free concentration of 2.5 mM. We have reported a maximum displacement of the total uptake of 50% with UCB-H, indicating that only about half of the total uptake is displaceable for [18F]UCB-H and therefore that BP_{ND} (k_3/k_4) would be expected close to 1.0, which is in agreement with the average value of 1.1 reported in Table 1. Lower BP_{ND} values were reported in humans (12), however the binding potentials were derived relative to the centrum semiovale and would likely be higher if calculated using the true V_{ND} (14). Finally, the displacement study with LEV evidenced its slower brain penetrance compared to UCB-H, with a displacement of the total uptake of ~ 40% measured 2.5 h after 30 mg/kg i.v. LEV administration, which would correspond to an occupancy of ~ 75–80% of SV2A in agreement with values in the literature (14, 24, 38). We observed some displacement in the white matter both with [19F]UCB-H and LEV. This is likely due to high spill-in from cortical regions rather than true specific signal in the white matter, as indicated by the uptake and V_T higher than expected (12). Here, we coregistered T_2-weighted MR-PET images to the Ballanger template (31) and used the inverse transformation to extract TACs from the PET images. Cynomolgus brains have relatively small white matter regions, with some inter-animal variability. Therefore, this approach appeared less precise to segment white matter regions and prone to partial volume effect, and as such, the current data set did not allow to use or evaluate the utility of the white matter as a reference region.

Altogether, our data confirm similar brain penetration and non-displaceable uptake for [18F]UCB-H as described for [11C]UCB-J (38), [18F]MNI1126 (16) (aka [18F]Synvest-1 (14)). In agreement with previous reports in rhesus NHP (23, 38), V_T-estimates and consequently BP_{ND} of [18F]UCB-H in cynomolgus NHP are considerably lower (~ 50% lower for V_T, and 3 to 4-fold lower for BP_{ND}) compared to V_T and BP_{ND} measures with [11C]UCB-J (35, 38) and other 18F-labelled SV2A radioligands, [18F]synvest1 (14, 16) and [18F]synvest2 (17) (alias [18F]SDM-2 (18)). As a consequence, [18F]UCB-H will be less sensitive to detect small changes compared to the latest SV2A ligands. Nevertheless, a clinical study using [18F]UCB-H in Alzheimer's Disease (AD) patients demonstrated a correlation between lower synaptic density and poorer awareness of memory functioning in Aβ-positive individuals (25), confirming earlier data in AD patients using [11C]UCB-J (41). Additionally, this

[18F]UCB-H clinical study (25) suggested a widespread synaptic decline in AD patients across the neocortex and in some subcortical nuclei, including the basal forebrain, which was confirmed in a comparable but larger cohort of AD patients using [11C]UCB-J (42). These and other data (21) demonstrate the potential of the [18F]UCB-H radioligand.

Conclusions

[18F]UCB-H was the first [18F]labeled SV2A radioligand (10, 11), before a long series of new [18F]labeled SV2A candidate ligands (17, 18, 24). Here, we aimed to complete existing data on [18F]UCB-H by pharmacokinetic studies in young NHP. We show that, when specific binding is low, a slow component gives rise to compartment modeling difficulties with k_4 close to 0, which has been previously reported for other SV2A candidate ligands (24, 39). Graphical analysis allows nevertheless a reliable quantification of V_T with acceptable aTRV and bias. Despite a lower sensitivity due to lower BP_{ND}, [18F]UCB-H recently provided sound data in a clinical AD study (25), paving the road for synaptic PET imaging using highly specific SV2A ligands in neurodegenerative disorders.

Abbreviations

1TCM One-compartment model

2TCM Two-compartment model

%SE Percentage standard error

AIC Akaike Information Criterion

aTRV Absolute Test-Retest variability

BP_{ND} Non-Displaceable Binding Potential

f_p Plasma parent

LEV Levetiracetam

mcAIF metabolite-corrected arterial plasma input function

NHP Non-human Primates

PET Positron Emission Tomography

TAC time-activity curves

SEM standard error of the mean

SUV standardized uptake value

VOI Volumes of interest

V_T Total Volume of Distribution

SV2A Synaptic vesicle glycoprotein 2A

Declarations

Ethics approval

Animal use procedures were in accordance with the recommendations of the European regulations (EU Directive 2010/63) and approved by the local ethical committee (CETEA n°44), and the French Ministry of Education and Research (NEUROMODEL: APAFIS#389-2015032716213569 0v02). The experimental data reported in this study are in compliance with the ARRIVE (Animal Research: Reporting in Vivo Experiments) guidelines (26).

Availability of data and material

The datasets used and/or analyzed during the current study are available from the corresponding author on reasonable request

Competing interests

None

Funding

This work was supported by NeurATRIS: A translational Research Infrastructure for Biotherapies in Translational Neurosciences (Investissement d'Avenir – ANR-11-INBS-0011, A.L.P.)

Authors' contributions

Radiochemistry: Guillaume Becker[3], Yann Bramoulle[1,2], , Christian Lemaire[3] **;** *Animal Experimentation:* Mylène Gaudin[1,2] , Martine Guillermier[1,2] **;** *PET Imaging:* Leopold Eymin[1,2], Nadja Van Camp[1,2]**;** *PET Modelling and Analysis:* Sébastien Goutal[1,2], Olivier Barret[1,2], Nadja Van Camp[1,2]*; Scientific writing:* Sébastien Goutal[1,2], Olivier Barret[1,2], Nadja Van Camp[1,2]**;** *Secured funding:* Philippe Hantraye[1,2] André Luxen[3], Alain Plenevaux

Acknowledgements

Authors are thankful to Leopold Eymin and Sophie Lecourtois for animal handling and PET acquisition. They also thank Romina Aron-Badin for animal care support and MRI acquisitions.

References

1. Bajjalieh SM, Frantz GD, Weimann JM, McConnell SK, Scheller RH. Differential expression of synaptic vesicle protein 2 (SV2) isoforms. The Journal of neuroscience : the official journal of the Society for Neuroscience. 1994;14(9):5223-35.
2. Janz R, Sudhof TC. SV2C is a synaptic vesicle protein with an unusually restricted localization: anatomy of a synaptic vesicle protein family. Neuroscience. 1999;94(4):1279-90.
3. Daniels V, Wood M, Leclercq K, Kaminski RM, Gillard M. Modulation of the conformational state of the SV2A protein by an allosteric mechanism as evidenced by ligand binding assays. British journal of pharmacology. 2013;169(5):1091-101.
4. Mendoza-Torreblanca JG, Vanoye-Carlo A, Phillips-Farfan BV, Carmona-Aparicio L, Gomez-Lira G. Synaptic vesicle protein 2A: basic facts and role in synaptic function. The European journal of neuroscience. 2013;38(11):3529-39.
5. Bartholome O, Van den Ackerveken P, Sánchez Gil J, de la Brassinne Bonardeaux O, Leprince P, Franzen R, et al. Puzzling Out Synaptic Vesicle 2 Family Members Functions. Frontiers in molecular neuroscience. 2017;10:148.
6. Loscher W, Gillard M, Sands ZA, Kaminski RM, Klitgaard H. Synaptic Vesicle Glycoprotein 2A Ligands in the Treatment of Epilepsy and Beyond. CNS drugs. 2016;30(11):1055-77.
7. Lynch BA, Lambeng N, Nocka K, Kensel-Hammes P, Bajjalieh SM, Matagne A, et al. The synaptic vesicle protein SV2A is the binding site for the antiepileptic drug levetiracetam. Proceedings of the National Academy of Sciences of the United States of America. 2004;101(26):9861-6.

8. Gillard M, Fuks B, Leclercq K, Matagne A. Binding characteristics of brivaracetam, a selective, high affinity SV2A ligand in rat, mouse and human brain: relationship to anti-convulsant properties. European journal of pharmacology. 2011;664(1-3):36-44.
9. Mercier J, Archen L, Bollu V, Carre S, Evrard Y, Jnoff E, et al. Discovery of heterocyclic nonacetamide synaptic vesicle protein 2A (SV2A) ligands with single-digit nanomolar potency: opening avenues towards the first SV2A positron emission tomography (PET) ligands. ChemMedChem. 2014;9(4):693-8.
10. Bretin F, Warnock G, Bahri MA, Aerts J, Mestdagh N, Buchanan T, et al. Preclinical radiation dosimetry for the novel SV2A radiotracer [18F]UCB-H. EJNMMI research. 2013;3(1):35.
11. Warnock GI, Aerts J, Bahri MA, Bretin F, Lemaire C, Giacomelli F, et al. Evaluation of 18F-UCB-H as a Novel PET Tracer for Synaptic Vesicle Protein 2A in the Brain. Journal of Nuclear Medicine. 2014;55(8):1336-41.
12. Bahri MA, Plenevaux A, Aerts J, Bastin C, Becker G, Mercier J, et al. Measuring brain synaptic vesicle protein 2A with positron emission tomography and [18 F]UCB-H. Alzheimer's & Dementia: Translational Research & Clinical Interventions. 2017;3(4):481-6.
13. Finnema SJ, Nabulsi NB, Eid T, Detyniecki K, Lin SF, Chen MK, et al. Imaging synaptic density in the living human brain. Science translational medicine. 2016;8(348):348ra96.
14. Naganawa M, Li S, Nabulsi NB, Henry S, Zheng MQ, Pracitto R, et al. First-in-human evaluation of (18)F-SynVesT-1, a novel radioligand for PET imaging of synaptic vesicle protein 2A. Journal of nuclear medicine : official publication, Society of Nuclear Medicine. 2020.
15. Mercier J, Provins L, Valade A. Discovery and development of SV2A PET tracers: Potential for imaging synaptic density and clinical applications. Drug discovery today Technologies. 2017;25:45-52.
16. Constantinescu CC, Tresse C, Zheng M, Gouasmat A, Carroll VM, Mistico L, et al. Development and In Vivo Preclinical Imaging of Fluorine-18-Labeled Synaptic Vesicle Protein 2A (SV2A) PET Tracers. Molecular imaging and biology : MIB : the official publication of the Academy of Molecular Imaging. 2018.
17. Cai Z, Li S, Zhang W, Pracitto R, Wu X, Baum E, et al. Synthesis and Preclinical Evaluation of an (18)F-Labeled Synaptic Vesicle Glycoprotein 2A PET Imaging Probe: [(18)F]SynVesT-2. ACS chemical neuroscience. 2020;11(4):592-603.
18. Cai Z, Li S, Finnema S, Lin S-f, Zhang W, Holden D, et al. Imaging synaptic density with novel 18F-labeled radioligands for synaptic vesicle protein-2A (SV2A): synthesis and evaluation in nonhuman primates. Journal of Nuclear Medicine. 2017;58(supplement 1):547.
19. Becker G, Dammicco S, Bahri MA, Salmon E. The Rise of Synaptic Density PET Imaging. Molecules (Basel, Switzerland). 2020;25(10).
20. Becker G, Warnier C, Serrano ME, Bahri MA, Mercier J, Lemaire C, et al. Pharmacokinetic Characterization of [(18)F]UCB-H PET Radiopharmaceutical in the Rat Brain. Molecular pharmaceutics. 2017;14(8):2719-25.
21. Serrano ME, Bahri MA, Becker G, Seret A, Mievis F, Giacomelli F, et al. Quantification of [(18)F]UCB-H Binding in the Rat Brain: From Kinetic Modelling to Standardised Uptake Value. Molecular imaging and biology : MIB : the official publication of the Academy of Molecular Imaging. 2018.
22. Serrano ME, Becker G. Evaluating the In Vivo Specificity of [(18)F]UCB-H for the SV2A Protein, Compared with SV2B and SV2C in Rats Using microPET. 2019;24(9).
23. Zheng M-Q, Holden D, Nabulsi N, Lin S-f, Mercier J, Hannestad J, et al. Synthesis and evaluation of 18F-UCB-H, a novel PET imaging tracer for the synaptic vesicle protein 2A. Journal of Nuclear Medicine. 2014;55(supplement 1):1792.
24. Constantinescu CC, Tresse C, Zheng M, Gouasmat A, Carroll VM, Mistico L, et al. Development and In Vivo Preclinical Imaging of Fluorine-18-Labeled Synaptic Vesicle Protein 2A (SV2A) PET Tracers. Mol Imaging Biol. 2019;21(3):509-18.
25. Bastin C, Bahri MA, Meyer F, Manard M, Delhaye E, Plenevaux A, et al. In vivo imaging of synaptic loss in Alzheimer's disease with [18F]UCB-H positron emission tomography. European journal of nuclear medicine and molecular imaging. 2020;47(2):390-402.

26. Kilkenny C, Browne WJ, Cuthill IC, Emerson M, Altman DG. Improving bioscience research reporting: the ARRIVE guidelines for reporting animal research. Osteoarthritis and cartilage. 2012;20(4):256-60.
27. Warnier C, Lemaire C, Becker G, Zaragoza G, Giacomelli F, Aerts J, et al. Enabling Efficient Positron Emission Tomography (PET) Imaging of Synaptic Vesicle Glycoprotein 2A (SV2A) with a Robust and One-Step Radiosynthesis of a Highly Potent (18)F-Labeled Ligand ([(18)F]UCB-H). Journal of medicinal chemistry. 2016;59(19):8955-66.
28. Goutal S, Langer O, Auvity S, Andrieux K, Coulon C, Caillé F, et al. Intravenous infusion for the controlled exposure to the dual ABCB1 and ABCG2 inhibitor elacridar in nonhuman primates. Drug delivery and translational research. 2018;8(3):536-42.
29. Van Camp N, Balbastre Y, Herard AS, Lavisse S, Tauber C, Wimberley C, et al. Assessment of simplified methods for quantification of [(18)F]-DPA-714 using 3D whole-brain TSPO immunohistochemistry in a non-human primate. Journal of cerebral blood flow and metabolism : official journal of the International Society of Cerebral Blood Flow and Metabolism. 2020;40(5):1103-16.
30. Tournier N, Cisternino S, Peyronneau MA, Goutal S, Dolle F, Scherrmann JM, et al. Discrepancies in the P-glycoprotein-mediated transport of (18)F-MPPF: a pharmacokinetic study in mice and non-human primates. Pharmaceutical research. 2012;29(9):2468-76.
31. Ballanger B, Tremblay L, Sgambato-Faure V, Beaudoin-Gobert M, Lavenne F, Le Bars D, et al. A multi-atlas based method for automated anatomical Macaca fascicularis brain MRI segmentation and PET kinetic extraction. NeuroImage. 2013;77:26-43.
32. Slifstein M, Laruelle M. Models and methods for derivation of in vivo neuroreceptor parameters with PET and SPECT reversible radiotracers. Nuclear medicine and biology. 2001;28(5):595-608.
33. Logan J, Fowler JS, Volkow ND, Wolf AP, Dewey SL, Schlyer DJ, et al. Graphical analysis of reversible radioligand binding from time-activity measurements applied to [N-11C-methyl]-(-)-cocaine PET studies in human subjects. Journal of cerebral blood flow and metabolism : official journal of the International Society of Cerebral Blood Flow and Metabolism. 1990;10(5):740-7.
34. Nicolas JM, Hannestad J, Holden D, Kervyn S, Nabulsi N, Tytgat D, et al. Brivaracetam, a selective high-affinity synaptic vesicle protein 2A (SV2A) ligand with preclinical evidence of high brain permeability and fast onset of action. Epilepsia. 2016;57(2):201-9.
35. Finnema SJ, Nabulsi NB, Mercier J, Lin SF, Chen MK, Matuskey D, et al. Kinetic evaluation and test-retest reproducibility of [(11)C]UCB-J, a novel radioligand for positron emission tomography imaging of synaptic vesicle glycoprotein 2A in humans. Journal of cerebral blood flow and metabolism : official journal of the International Society of Cerebral Blood Flow and Metabolism. 2017:271678x17724947.
36. Mansur A, Rabiner EA, Comley RA, Lewis Y, Middleton LT, Huiban M, et al. Characterization of 3 PET Tracers for Quantification of Mitochondrial and Synaptic Function in Healthy Human Brain: (18)F-BCPP-EF, (11)C-SA-4503, and (11)C-UCB-J. Journal of nuclear medicine : official publication, Society of Nuclear Medicine. 2020;61(1):96-103.
37. Li S, Cai Z, Wu X, Holden D, Pracitto R, Kapinos M, et al. Synthesis and in Vivo Evaluation of a Novel PET Radiotracer for Imaging of Synaptic Vesicle Glycoprotein 2A (SV2A) in Nonhuman Primates. ACS Chem Neurosci. 2019;10(3):1544-54.
38. Nabulsi NB, Mercier J, Holden D, Carré S, Najafzadeh S, Vandergeten M-C, et al. Synthesis and Preclinical Evaluation of 11C-UCB-J as a PET Tracer for Imaging the Synaptic Vesicle Glycoprotein 2A in the Brain. Journal of Nuclear Medicine. 2016;57(5):777-84.
39. Estrada S, Lubberink M, Thibblin A, Sprycha M, Buchanan T, Mestdagh N, et al. [(11)C]UCB-A, a novel PET tracer for synaptic vesicle protein 2A. Nuclear medicine and biology. 2016;43(6):325-32.
40. Patel S, Knight A, Krause S, Teceno T, Tresse C, Li S, et al. Preclinical In Vitro and In Vivo Characterization of Synaptic Vesicle 2A-Targeting Compounds Amenable to F-18 Labeling as Potential PET Radioligands for Imaging of Synapse Integrity. Molecular imaging and biology : MIB : the official publication of the Academy of Molecular Imaging. 2020;22(4):832-41.

41. Chen MK, Mecca AP, Naganawa M, Finnema SJ, Toyonaga T, Lin SF, et al. Assessing Synaptic Density in Alzheimer Disease With Synaptic Vesicle Glycoprotein 2A Positron Emission Tomographic Imaging. JAMA neurology. 2018.
42. Mecca AP, Chen MK, O'Dell RS, Naganawa M, Toyonaga T, Godek TA, et al. In vivo measurement of widespread synaptic loss in Alzheimer's disease with SV2A PET. Alzheimer's & dementia : the journal of the Alzheimer's Association. 2020.

Figures

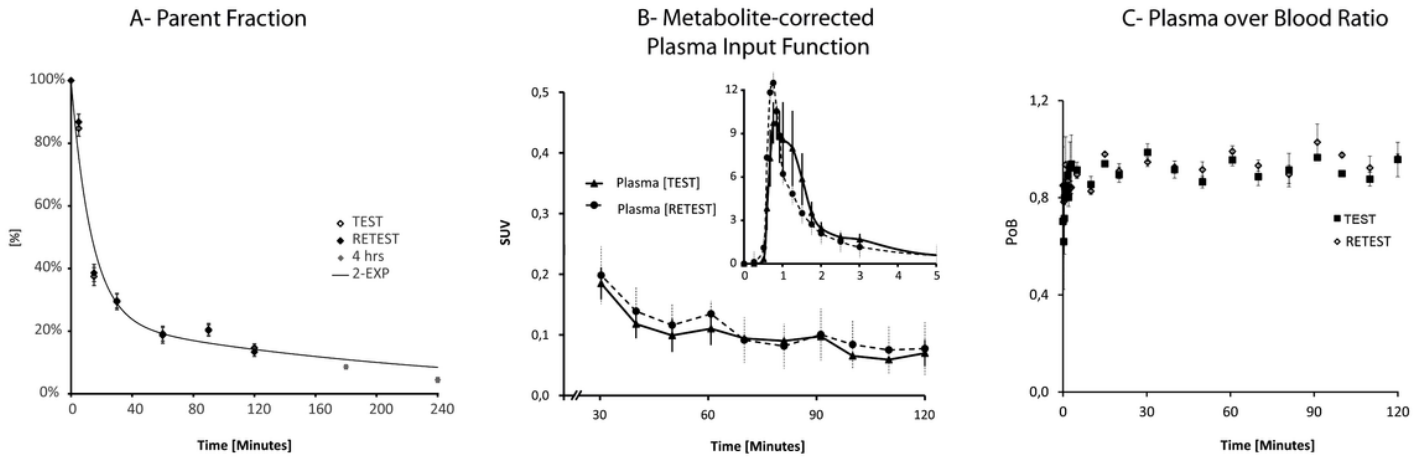

Figure 1

Blood measures after i.v. [18F]UCB-H injection in the cynomolgus NHP. A- Parent fraction (in %) of [18F]UCB-H of test- and retest scans; B- Average (±SEM) metabolite-corrected plasma input function of test- and retest scans. C- Plasma to whole blood ratio of [18F]UCB-H over time of test- and retest scans.

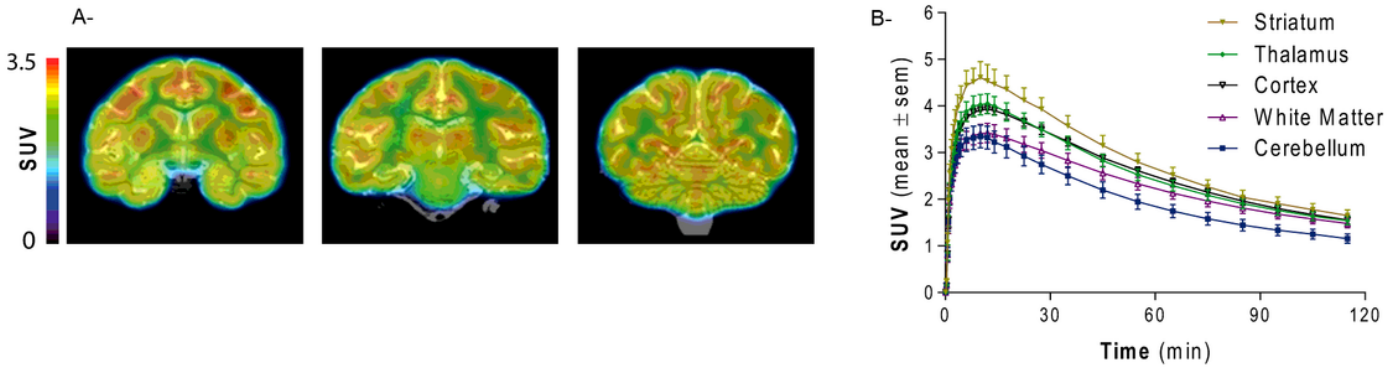

Figure 2

A- Representative 60-120 min summed PET / T2-weighted MR images. B- Average (±SEM) TAC in striatum, thalamus, cortex, white matter and cerebellum.

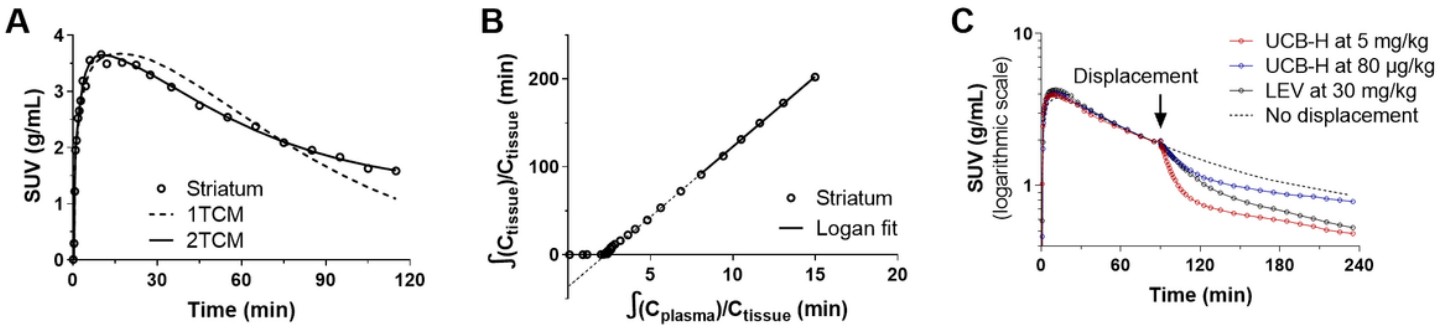

Figure 3

A- Striatal TAC (circles) fitted against 1TCM (dashed line) and 2TCM (full line); B- Logan graphical linear fit of striatal TAC (circles) with t* fixed at 60 min. C- Displacement of [18F]UCB-H at 90 min after radioligand injection by LEV at 30mg/kg (black), [19F]UCB-H at 80 µg/kg (red) and 5 mg/kg (blue). The displacement studies TACs are normalized to the baseline value just before displacement.

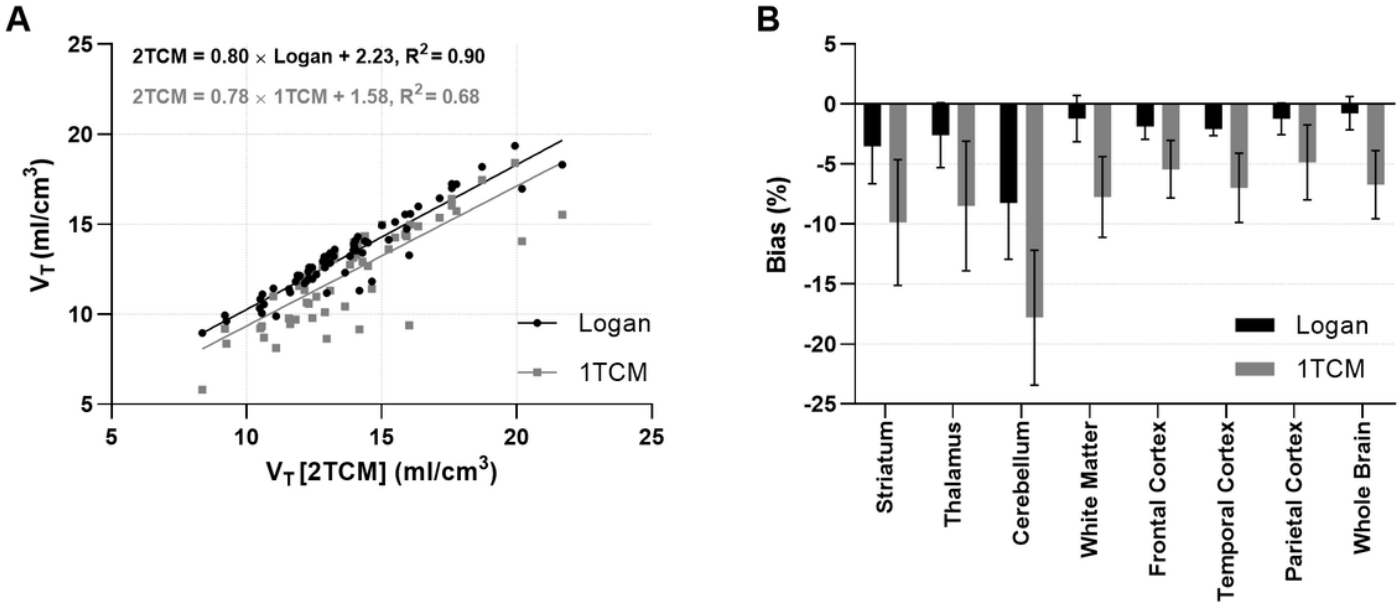

Figure 4

A- Linear correlations between VT obtained with 2TCM, and Logan or 1TCM. B- Bias of Logan and 1TCM VT estimates compared to 2TCM in several brain regions.